Natural Hazards and Earth System Sciences

Open Access

Discussions

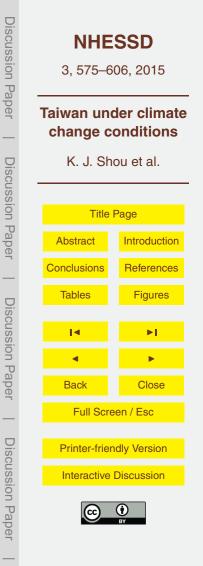# Predictive analysis of landslide susceptibility in the Kao-Ping watershed, Taiwan under climate change conditions

K. J. Shou, C. C. Wu, and J. F. Lin

Department of Civil Engineering, National Chung-Hsing University 250, Kuo-Kuang Road, Taichung, Taiwan

Correspondence to: K. J. Shou (kjshou@dragon.nchu.edu.tw)

Discussion Paper | Discussion Paper | Discussion Paper | Discussion Paper

NHESSD

3, 575–606, 2015

Taiwan under climate change conditions

K. J. Shou et al.

Title Page

Abstract | Introduction

Conclusions | References

Tables | Figures

◀◀ | ▶▶

◀ | ▶

Back | Close

Full Screen / Esc

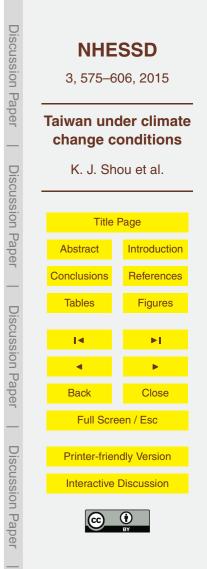Printer-friendly Version

Interactive Discussion

Abstract

Among the most critical issues, climatic abnormalities caused by global warming also affect Taiwan significantly for the past decade. The increasing frequency of extreme rainfall events, in which concentrated and intensive rainfalls generally cause geohazards including landslides and debris flows. The extraordinary Typhoon Morakot hit Southern Taiwan on 8 August 2009 and induced serious flooding and landslides. In this study, the Kao-Ping River watershed was adopted as the study area, and the typical events 2007 Krosa Typhoon and 2009 Morakot Typhoon were adopted to train the susceptibility model. This study employs rainfall frequency analysis together with the atmospheric general circulation model (AGCM) downscaling estimation to understand the temporal rainfall trends, distributions, and intensities in the Kao-Ping River watershed. The rainfall estimates were introduced in the landslide susceptibility model to produce the predictive landslide susceptibility for various rainfall scenarios, including abnormal climate conditions. These results can be used for hazard remediation, mitigation, and prevention plans for the Kao-Ping River watershed.

1 Introduction

Due to the climatic abnormalities in the past decade, Taiwan has been significantly affected by the concentrated rainfall periods and high rainfall intensities. The frequency of extreme events is increasing, which subsequently increases the risk of natural hazards. With the majority of its geologically young strata fractured by the plate tectonic activities, in addition to the nature of rapid river morphological changes, it is particularly prone to landslides and debris flows during periods of torrential rain, especially in the west foothill of Taiwan Island. The Kao-Ping River watershed, one of the major watersheds prone to geohazards in southern Taiwan, was adopted as the study area (see Fig. 1). Although there are studies on the landslides in this area, especially after the 2009 Morakot typhoon (Chen et al., 2011; Lin et al., 2011, 2014; Tsou et al.,

2011; Shou, 2013), the impact of the climatic abnormalities is seldom considered in the landslide analysis, which motivates this study.
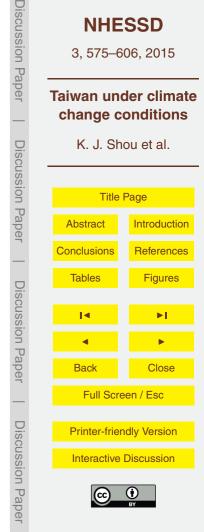
This study aimed to determine future changes in rainfall caused by climate change as a basis for the analysis of landslide susceptibility. This study used SPOT satellite images to calculate a normalized difference vegetation index (NDVI) and identified landslides in the Kao-Ping River watershed during 2007 Typhoon Krosa and 2009 Typhoon Morakot. The data of these two typhoons were used to train the susceptibility model. And the logistic regression model was compared with the instability index method before adopted for the predictive landslide susceptibility analysis.

In this study, slope angle, aspect, elevation, dip slope index (I_{ds}), distance to the road, distance to river, distance to fault, and landslide-rainfall index (I_d) were selected as the control factors. In addition, rainfall data estimated by the rainfall frequency analysis and the dynamic downscaling global circulation model were used for the predictive landslide susceptibility analyses.

2 Basics of the study area

2.1 Geological background

The Kao-Ping River catchment traverses two geological regions, including the alluvial plain and the Central Range of Taiwan Island (Ho, 1994). Since the Kao-Ping River flows from the northeast to the southwest and the linear structures mainly trend in the north–south direction, the Kao-Ping River crosses several sedimentary and metamorphic formations with different geological ages. Due to the vibrant tectonic activities, a series of imbricated structures (including folds and faults) were formed in the north–south direction. The major faults from the west to the east include Chaochou fault, Ailiao fault and Shiaotushan fault (see Fig. 1).
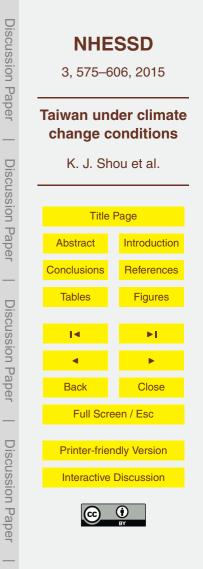
2.2 Automatic identification of landslide

To identify landslides, this study used SPOT satellite images to obtain NDVI data and used 5 m digital terrain model (DTM) to obtain slope angle data. The two data layers, together with properly chosen threshold values, were used to identify the landslides automatically. The interpretation results from various NDVI and slope angle thresholds were compared with the landslide inventories provided by the Central Geological Survey of Taiwan. According to a preliminary comparison study (Wu, 2013), the most accurate threshold combination of NDV I = 0.0 and slope = 40 % was adopted in this study. In addition, the influences of shadows in the satellite images were further treated before the automatic identification of landslides.

NDVI suffers from the poor spectral resolution in the shadow areas where most objects appear greyish so that the NDVI tends to 0. Therefore, the landslides detected by NDVI might be overestimated in the shadow areas (Beumier and Idrissa, 2014). Different screening indexes, including brightness (Hsieh et al., 2011), greenness (Liu et al., 2012; Lin et al., 2013), and vegetation mask (Beumier and Idrissa, 2014), were coupled with the NDVI criteria to improve the accuracy of landslide identification in shadow areas. Based on the suggestions of Lin et al. (2013) and Chen (2014), the greenness of 0.14 was adopted as the screening criterion in this study. The performance of the additional greenness criterion is shown in Table 1.

The comparison in Table 1 is based on the landslide inventories of 2007 Krosa and 2009 Morakot provided by the Central Geology Survey of Taiwan. The results in Table 1 also reveal that the accuracy is lower for 2009 Morakot, especially for the group of landslide cells. The reason could be the 2009 Morakot generated more landslides with lower slope, which cannot be totally interpreted by the criterion. The landslide identification accuracy of the total cells is reasonably good; therefore, the adopted slope-NDVI-greenness criterion can be applied in the study area in the future.
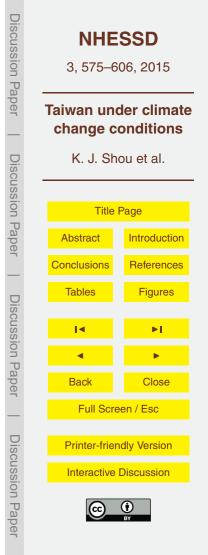
2.3   The control factors of landslide

To examine the correlation between the major control factors and the landslide susceptibility, this study reviewed the references of rainfall-induced landslides (Selby, 1993; Süzen and Doyuran, 2004; Hsu, 2007; Hong, 2010; Rossi et al., 2010) and adopted eight landslide control factors, that is, slope degree, aspect, dip slope index (I_{ds}), distance from the road, water system, distance to fault, elevation, and landslide-rainfall index (I_d). The data layers of those control factors were applied for the susceptibility analysis by geographic information system (GIS). Among the other common factors, for clarity, the dip slope index and the landslide-rainfall index are defined as below.

The dip slope index (I_{ds}) is defined as the angle difference between the dip direction of weak planes (bedding planes or joints) and the dip direction of the slope, where the resulting angles are classified as a highly-dip slope (± 0–$\pm 30°$), medium-dip slope (± 30–$\pm 60°$), orthoclinal slope (± 60–$\pm 120°$), medium-reverse slope (± 120–$\pm 150°$), and highly-reverse slope (± 150–$\pm 180°$). This index can reflect the tendency of dip slope failure.

Considering the rainfall induced landslides, accumulative rainfall and rainfall intensity are all important control factors. However, they are highly correlated especially for the rainfalls of typhoons. In this study, the landslide-rainfall index (I_d) was introduced to accommodate these two interdependent control factors. Figure 2 illustrates the correlation between accumulated rainfall and rainfall intensity (we adopt maximum hourly rainfall as the rainfall intensity in this study) of the landslide locations. We can graphically obtain the upper and lower boundary linear thresholds from this graph. Such that the distances from the unknown point (to determine the landslide susceptibility with known rainfall data) to the upper and lower thresholds, i.e., the values d_1 and d_2, can be determined. The landslide-rainfall index (I_d) is defined as

$$I_d = d2/(d1 + d2) \tag{1}$$

The landslide-rainfall index (I_d) ranges between 0 and 1. As I_d approaches 1, the slope becomes increasingly susceptible to rainfall-induced landslide. On the contrary, as the

point of the rainfall of potential landslide approaches the lower threshold, or as I_d approaches 0, the slope becomes less susceptible to rainfall-induced landslide.

3   Susceptibility analysis methods

3.1   Instability Index Method

Instability Index Method (IIM), also called Multiple Nonlinear Regression Analysis, or Dangerous Value Method, which is proposed by Jian (1992). IIM describes the unstable degree of slopes by some landslide causative factors (D). IIM has no input number limit, and any type (continuous or discontinuous) of landslide causative factors can be accepted; and this is the most advantage of IIM. The processing steps of IIM are: first, divided each factor into several ranks, and then sequentially calculated the landslide density (G_i) in grid based, the proportion of failure (S_i) for every rank. The normalized grades (D_i) defines as:

$$D_i = \frac{9\,(X_i - X_{min})}{(X_{max} - X_{min})} + 1 \tag{2}$$

in which X_{min} is the minimum value of proportion of failure and X_{max} is the maximum value of proportion of failure.

The weighting value w_i of the ith factor is defined as the ratio of individual variation coefficient with the sum of all factors', representing as the following formula

$$w_i = \frac{V_i}{(V_1 + V_2 + \ldots + V_n)} \tag{3}$$

v_i represents coefficient of variation of the ith factor In this model, we need to consider unbiasedness, so that the total weight must be equal to unity, i.e., the values of weighting number (w_i, $i = 1 \sim n$) are all less than 1, their sum equals 1.

After we get the landslide susceptibility index P ($P \in (0,1)$), a normalized value of the total instability index number D_{total}, which includes the influence of all control factors. The instability index I_P is defined in terms of weighting values w_i ($i = 1 \sim n$) and grading values D_i ($i = 1 \sim n$) of all control factors as

$$I_P = \log(D_{total}) = \log\left(D_1^{w_1} \times D_2^{w_2} \times \ldots \times D_n^{w_n}\right) \tag{4}$$

It is worth noting that the value of D_{total} is between 1 and 10 and the value of P is between 0 and 1. The higher the values of D_{total} and P, the higher the landslide susceptibility. It is an index for the probability of landslide, i.e., the potential of landslide hazards.
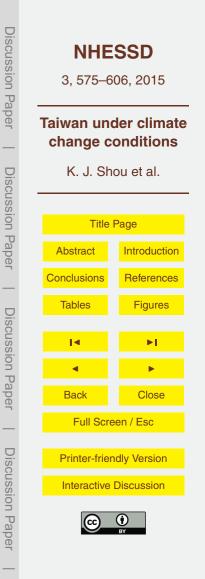
3.2 Logistic regression method

In this study, the method of logistic regression (LRM) was adopted to analyze the landslide susceptibility. Based on the training samples, which comprised a group of data points or data locations, categorized as landslide and non-landslide. The data layer of each factor was then placed upon the landslide and non-landslide layers, and the correlation between each factor and landslides was used to conduct binary logistic regression (Atkinson and Massari, 1998; Süzen and Doyuran, 2004; Lee et al., 2008; Mathew et al., 2009; Rossi et al., 2010; Akgun, 2012; Lee, 2012; Devkota, 2013).

The logistic regression model is a form of the logarithmic linear model where the dependent variable is binary. This model can be expressed as

$$\ln\left[\frac{P_i}{1 - P_i}\right] = \alpha + \sum_{i=1}^{k} \beta_k x_{ki} \tag{5}$$

where $P_i = P(y_i = 1 | x_{1i}, x_{2i}, \ldots x_{ki})$ and represents the probability of an event occurring when a series of given independent variables are equal to $x_{1i}, x_{2i}, \ldots x_{ki}$, and α and β_k are the constants. In the landslide susceptibility analysis, the probability $P_i = 1$ for the

landslide points, and the probability $P_i = 0$ for the non-landslide points. Coefficients α, β_k can be obtained following the regression of training data.

This study employed the receiver operating characteristic (ROC) curve (Swets, 1988) and the success rate (SR) curve (Chung and Fabbri, 2003) to verify the model. The area under the curve (AUC) of the ROC curve or the SR curve can be used to evaluate the prediction accuracy of a susceptibility model. Generally, the larger the AUC values the better. As the area approaches 0.5, the result may not necessarily be superior to that of a random selection. AUC values of less than 0.5 are not worth employing.
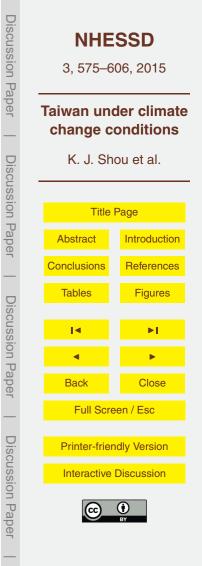
4 Rainfall estimation

This study used the method of Kriging to estimate the spatial distributions of rainfalls. The estimation of rainfalls primarily emploies (1) historical data and rainfall frequency analysis and Eq. (1) the climate change model estimates.

4.1 Rainfall frequency analysis

The rainfall data from the 7 weather monitoring stations of the Central Weather Bureau in the Kuo-Ping River watershed was collected for the rainfall analysis and prediction (see Fig. 1). The K-S (Kolmogorov–Smirnovest) test was employed to eliminate unsuitable distributions, and the standard error was used to select the optimal rainfall distribution for each station.

According to the studies of Hong (2010) and Shou (2011) on the rainfall frequency in Taiwan area, the Hazen method (Kadoya, 1992; Hosking and Wallis, 1997; Castellarina et al., 2009; El Adlouni and Ouarda, 2010) was adopted for the return period frequency analysis. The obtained frequency analysis model was used to predict the rainfall (maximum hourly rainfall, accumulative annual precipitation, and 24, 48, and 72 h accumulative rainfall) in the Kao-Ping River watershed for the return periods of 10, 20, and 100 years.

The results of the rainfall frequency analysis for each station, i.e., the rainfall values for different return periods, were interpolated using the Geostatistical Analyst Kriging function of the GIS. We can determine the spatial distributions of rainfall intensity and accumulative rainfall for various return periods in the Kao-Ping River watershed (see Figs. 3 and 5).
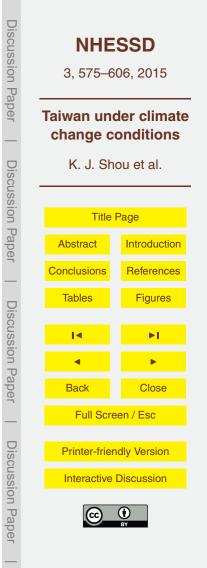
4.2 The climate change models for rainfall estimates

The Taiwan Climate Change Projection and Information Platform Project (TCCIP), analyzes the results from the assessment reports of the United Nations Intergovernmental Panel on Climate Change (IPCC), intended to assess the information concerning climate change, including the scientific and socio-economic information, its potential effects of, and the options for management and mitigation (IPCC, 2013; TCCIP, 2013). TCCIP applied the method of statistical downscaling to 24 Global Climate Models (GCMs) from the IPCC assessment report to obtain regionally downscaled results for Taiwan. The predictive rainfall data in this study was provided by the TCCIP, which uses the high-resolution climate simulation of MRI-JMA AGCM (Matsueda et al., 2009) as the initial and boundary conditions for the dynamical downscaling to produce 5 km high-resolution climate simulations of the near future (2015–2039) and the far future (2075–2099).

MRI-JMA AGCM was developed based on the numerical model used by the Japan Meteorological Agency for weather forecasts. With a horizontal resolution of approximately 20 km, the MRI-JMA AGCM is a super high-resolution global model (Matsueda et al., 2009). The model simulates climate estimates for three time periods, i.e., the present (1979–2003), the near future (2015–2039), and the far future (2075–2099). For the future emission consideration of the IPCC data, this study adopted the Scenarios A1B which emphasizes economic growth and a convergence of global socioeconomic conditions (IPCC, 2013). The ocean–atmosphere general circulation modeling with A1B scerinio suggests that sea-surface temperatures (SST) exhibit a linearly in-

creasing trend. The variation of present SST was added to the linearly increasing SST for the AGCM estimation.

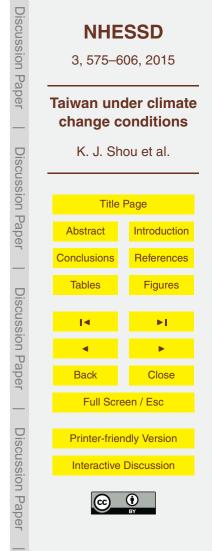The estimation of MRI-JMA AGCM (Matsueda et al., 2009) was used as the initial and boundary conditions for the dynamic downscaling. The regional model adopted to execute dynamic downscaling was the Weather Research and Forecasting (WRF) modeling system developed by the National Center for Atmospheric Research (NCAR). By the coupled MRI-AGCM dynamic downscaling approach, we can estimate the seasonal rainfall changes in Taiwan at the end of the twenty-first century (TCCIP, 2013). Based on the MRI-WRF dynamical downscaling data provided by TCCIP, we can estimate the future distributions of rainfalls with the consideration of climate change. Kriging interpolation was conducted on the data of the thirty five $5\,km \times 5\,km$ domains within the Kao-Ping River watershed to estimate the distribution of accumulative rainfall and rainfall intensity of the future (see Figs. 6 and 7).

5 Results

Considering the comparison basis and future applicability of landslide susceptibility model, this study adopted landslide interpreted by the same slope-NDVI-greenness criterion for 2007 Krosa and 2009 Morakot. Based on the obtained databases and the methodologies described in the previous sections, the landslide susceptibility analysis was performed. The data layers of the control factors based on the collected geology, topography, and rainfall data were generated and illustrated in Fig. 8.

5.1 Landslide susceptibility analysis

After normalizing the values of control factors of the landslide groups, we can obtain the data layers for the logistic regression analysis, which can be performed by the SPSS software.

The results of the instability index analysis can be expressed as below:

$$I_P = F_1^{0.101} \times F_2^{0.115} \times F_3^{0.081} \times F_4^{0.156} \times F_5^{0.098} \times F_6^{0.255} \times F_7^{0.118} \times F_8^{0.078} \quad (6)$$

for 2001 Krosa typhoon, and

$$I_P = F_1^{0.115} \times F_2^{0.095} \times F_3^{0.064} \times F_4^{0.152} \times F_5^{0.127} \times F_6^{0.250} \times F_7^{0.099} \times F_8^{0.099} \quad (7)$$

for 2009 Morakot typhoon, where I_P is the instability index, F_1 is the slope angle, F_2 is the elevation, F_3 is the aspect, F_4 is the distance to fault, F_5 is the distance to river, F_6 is the distance to road, F_7 is the dip slope index (I_{ds}), and F_8 is the landslide-rainfall index (I_d). The landslide susceptibility maps induced by Krosa and Morakot using Eqs. (6) and (7) are shown in Fig. 9.

The results of logistic regression analysis can be expressed as below:

$$\ln\left[\frac{P}{1-P}\right] = 0.844F_1 - 0.371F_2 - 0.361F_3 - 0.318F_4 - 0.438F_5 + 0.363F_6$$
$$- 0.206F_7 + 0.477F_8 - 0.096 \quad (8)$$
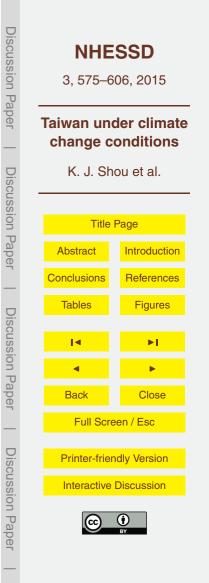
for 2001 Krosa typhoon, and

$$\ln\left[\frac{P}{1-P}\right] = 0.953F_1 + 0.107F_2 - 0.242F_3 - 0.106F_4 - 0.500F_5 + 0.217F_6$$
$$- 0.197F_7 + 0.240F_8 - 0.077 \quad (9)$$

for 2009 Morakot typhoon. In which P is the logistic function, $F_1 \sim F_8$ are the same control factors defined previously. The landslide susceptibility maps induced by Krosa and Morakot using Eqs. (8) and (9) are shown in Fig. 10.

Figures 9 and 10 reveal that a larger area with high landslide susceptibility during Morakot than during Krosa, indicates that Typhoon Morakot generated more severe landslides in the Kao-Ping River watershed. The landslide susceptibility models were
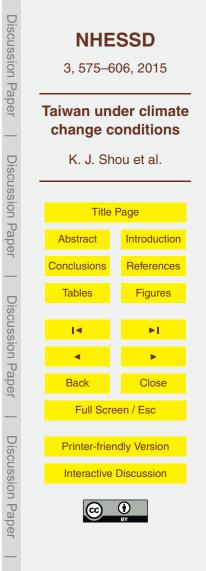
verified using the AUC values of the ROC curves. The results in Figs. 11 and 12 show that the AUC values of the instability index method are 0.655 for 2007 Krosa and 0.620 for 2009 Morakot, and the AUC values of the logistic regression method is 0.680 for 2007 Krosa and 0.672 for 2009 Morakot. For both typhoon events, the logistic regres-
5 sion method can obtain higher AUC values. Although the results suggest that the logistic regression susceptibility models with Eqs. (8) and (9) are all reasonable and acceptable, the model with higher AUC value, i.e. the Eq. (8) of 2007 Krosa was adopted for the predictive landslide analyses.

5.2 Landslide susceptibility predictions

10 Introducing the results of rainfall frequency analysis (Figs. 3 and 4 into the landslide susceptibility model, 9 rainfall scenarios (24, 48, and 72 h with return periods of 10, 20, and 100 years) can be analyzed. It should be noted that, due to the length limitation of the paper, only the major landslide susceptibility maps with the predicted rainfall scenarios were included. The major landslide susceptibility distributions for various
15 return periods are shown in Figs. 13 and 14. The results in Figs. 13 and 14 show that the longer the rainfall the more the landslide susceptibility, and the longer the return period the more the landslide susceptibility. In other words, the area with higher landslide susceptibility will increase if the rainfall is longer or the return period is longer.

The rainfalls predicted by the climate change dynamic downscaling method (Figs. 6
20 and 7) can also be introduced to the landslide susceptibility model. It can help to identify the potential landslide hazards in the near future (2015–2039) and in the far future (2075–2099). The results in Figs. 16 and 17 suggest that the landslide susceptibility is higher in the far future (2075–2099) than in the near future (2015–2039). And the high landslide susceptibility area increases significantly in the up-stream area, i.e., the
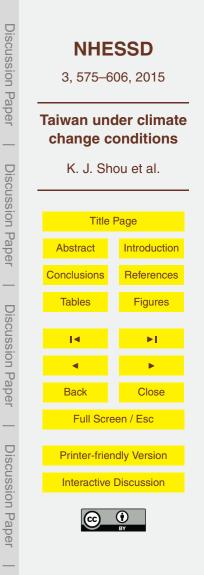25 southeast side of the watershed.

6 Conclusions and suggestions

In this study, focusing on the Kao-Ping watershed, predictive analyses of landslide susceptibility were performed with the consideration of climate change. Based on the training with the data of 2007 Krosa and 2009 Morakot, the logistic regression landslide susceptibility model was developed. The AUC of the model is in the level of $0.65 \sim 0.70$, which indicates its applicability for identify potential landslides.

The susceptibility maps calculated by the susceptibility model all showed that the mid-upstream and up-stream areas of the Kao-Ping River were highly susceptible to landslides. The predictive susceptibility analyses suggest that the new high landslide susceptibility areas are mainly distributed in the upstreams, including the south side and the southeast side of the watershed. The southeast side of the watershed is more critical because the analysis results of the far future also reveal the same finding.

The prediction capability of the susceptibility model is influenced by the weight of landslide-inducing factors, the limit of these factors (e.g. I_d has a maximum value of 1), and rainfall distributions. Therefore, the model's prediction ability is limited. More modification of the susceptibility based on more training data is essential to improve the accuracy. This study used rainfall frequency analysis and AGCM to estimate rainfall and predict future rainfall trends and intensity under climate change conditions. Rainfall frequency analysis with more data and a better AGCM can help to obtain a better rainfall estimation to more accurately predict the landslide susceptibility. The slope-NDVI-greenness criterion can identify landslides with an acceptable accuracy, however, the interpretation accuracy of landslide cells is still improvable, especially for the extreme events. More effort is suggested for a better landslide interpretation accuracy (Martha et al., 2010).

Printer-friendly Version

Interactive Discussion

References

Akgun, A.: A comparison of landslide susceptibility maps produced by logistic regression, multi-criteria decision, and likelihood ratio methods: a case study at Izmir, Turkey, Landslides, 9, 93–106, 2012.

Atkinson, P. M. and Massari, R.: Generalized linear modelling of susceptibility to landsliding in the central Apennines, Italy, Comput. Geosci., 24, 373–385, 1998.

Beumier, C. and Idrissa, M.: Building detection with multi-view colour infrared imagery, EARSeL eProceedings, 13, 77–84, 2014.

Castellarina, A., Merz, R., and Blöschl, G.: Probabilistic envelope curves for extreme rainfall events, J. Hydrol., 378, 263–271, 2009.

Chen, C. H., Tan, C. H., Chi, S. Y., and Su, T. W.: Application of GIS-based deterministic model for assessment of regional rainfall-induced landslide potential-example of Kao-Ping river watershed, J. Chinese Soil Water Conserv., 42, 1–11, 2011.

Chen, W. J.: On The Satellite Automatic Interpretation and Susceptibility Analysis of Shallow and Deap-Seated Landslide – A Study of Li-Shing Estate Road, Master thesis, NCHU, Taichung, Taiwan, 2014 (in Chinese).

Chung, C. F. and Fabbri, A. G.: Probabilistic prediction models for landslide hazard mapping, Photogramm. Eng. Rem. S., 65, 1389–1399, 2003.

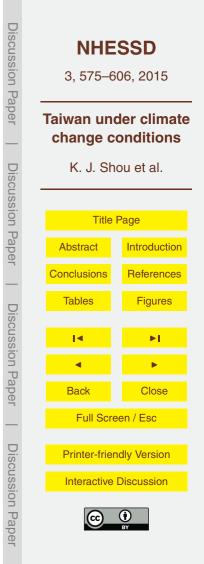Devkota, K. C.: Landslide susceptibility mapping using certainty factor, index of entropy and logistic regression models in GIS and their comparison at Mugling-Narayanghat Road section in Nepal Himalaya, Nat. Hazards, 65, 135–165, 2013.

El Adlouni, S. and Ouarda, T. B. M. J.: Frequency Analysis of extreme rainfall events, in: Rainfall: State of the Science, Geophys. Monogr. Ser., Vol. 191, AGU, Washington DC, 287 pp., 2010.

Ho, C. S.: Introduction to the Geology of Taiwan, 2nd Edn., Central Geological Survey, Taiwan, 1994.

Hong, C. Y.: Time Series Analysis of the Control Factors of the Landslides in Central Taiwan Area, Master thesis, NCHU, Taichung, Taiwan, 2010 (in Chinese).

Hosking, J. R. M. and Wallis, J. R.: Regional Frequency Analysis, Cambridge University Press, 1997.

Hsieh, Y. T., Wu, S. T., Liao, C. S., Yui, Y. G., Chen, J. C., and Chung, Y. L.: Automatic extraction of shadow and non-shadow landslide area from ADS40 image by stratified classification,

Geoscience and Remote Sensing, IEEE International Symposium – IGARSS, 3050–3053, Vancouver, 24–29 July, 2011.

Hsu, H. Y.: On the Control Factors of the Rainfall-induced Landslides in Central Taiwan Area, Master thesis, NCHU, Taichung, Taiwan, 2007 (in Chinese).

IPCC: Fifth Assessment Report: Climate Change (AR5), Switzerland, 2013.

Jian, L. B.: Application of Geographic Information System in the Quantitative Assessment of Slope Stability, MS thesis, NCHU, Taichung, Taiwan, 1992 (in Chinese).

Kadoya, M.: Study on record flood peaks in Japan, Proc. Jpn Acad. Ser. B 68, 133–138, 1992.

Lee, C. T.: Characteristics of earthquake-induced landslides and differences compared to storm-induced landslides, Geophys. Res. Abstracts, 14, EGU2012-6937-2, 6937 pp., 2012.

Lee, C. T., Huang, C. C., Lee, J. F., Pan, K. L., Lin, M. L., and Dong, J. J.: Statistical approach to earthquake induced landslide susceptibility, Eng. Geol., 100, 43–58, 2008.

Lin, C. W., Chang, W. S., Liu, S. H., Tsai, T. T., Lee, S. P., Tsang, Y. C., Shieh, C. L., and Tseng, C. M.: Landslides triggered by the 7 August 2009 typhoon Morakot in southern Taiwan, Eng. Geol., 123, 3–12, 2011.

Lin, E. J., Liu, C. C., Chang, C. H., Cheng, I. F., and Ko, M. H.: Using the FORMOSAT-2 high spatial and temporal resolution multispectral image for analysis and interpretation of landslide disasters in Taiwan, J. Photogramm. Rem. S., 17, 31–51, 2013.
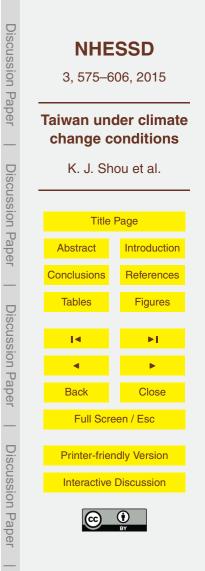
Lin, M. L., Chen, T. W., Lin, C. W., Ho, D. J., Cheng, K. P., Yin, H. Y., and Chen, M. C.: Detecting large-scale landslides using Lidar data and aerial photos in the Namasha-Liuoguey area, Taiwan, Remote Sens., 6, 42–63, 2014.

Liu, J. K., Hsiao, K. H., and Shih, T. Y.: A geomorphological model for landslide detection using airborne LIDAR data, J. Mar. Sci. Technol., 20, 629–638, 2012.

Martha, T. R., Kerle, N., Jetten, V., van Westen, C. J., and Kumar, K. V.: Characterising spectral, spatial and morphometric properties of landslides for semi-automatic detection using object-oriented methods, Geomorphology, 116, 24–36, 2010.

Mathew, J., Jha, V. K., and Rawat, G. S.: Landslide susceptibilityzonation mapping and its validation in part of Garhwal LesserHimalaya, India, using binary logistic regression analysis and re-ceiver operating characteristic curve method, Landslides, 6, 17–26, 2009.

Matsueda, M., Mizuta, R., and Kusunoki, S.: Future change in wintertime atmospheric blocking simulated using a 20-km-mesh atmospheric global circulation model, J. Geophys. Res.-Atmos., 114, D12114, doi:10.1029/2009JD011919, 2009.

Rossi, M., Guzzetti, F., Reichenbach, P., Mondini, A. C., and Peruccacci, S.: Optimal landslide susceptibility zonation based on multiple forecasts, Geomorphology, 114, 129–142, 2010.

Selby, M. J.: Hillslope Materials and Processes, Oxford University Press, New York, 1993.

Shou, K. J.: On the Spatial and Temporal Susceptibility Analysis of Landslide Hazard, report of National Science Council, Taiwan, 2011.

Shou, K. J.: Analysis of the Landslide Susceptibility in Kao-Ping River Watershed and Wu River Watershed, Taiwan, Seminar of CNR IRPI, 24 September 2013, Perugia, Italy, 2013.

Süzen, M. L. and Doyuran, V.: A comparison of the GIS based land-slide susceptibility assessment methods: multivariate vs. bi-variate, Environ. Geol., 45, 665–679, 2004.

Swets, J. A.: Measuring the accuracy of diagnostic systems, Science, 240, 1285–1293, 1988.

TCCIP: Development of Information Platform for Climate Change Estimation of Taiwan, National Science Council, Taiwan, 2013.

Tsou, C. Y., Feng, Z. Y., and Chigira, M.: Catastrophic landslide induced by Typhoon Morakot, Shiaolin, Taiwan, Geomorphology, 127, 166–178, 2011.

Yang, M. S, Lin, M. C., and Liu, J. K.: Integrating geomorphic indexes and SPOT multispectral imagery for landslides classification, J. Photogramm. Rem. S., 14, 11–23, 2009.

Wu, C. T.: Temporal and Spatial Landslide Susceptibility Analysis of the Kao-Ping Watershed, Master thesis, NCHU, Taichung, Taiwan, 2013 (in Chinese).

Table 1. The accuracy of landslide interpretation by the slope-NDVI-greenness criterion.

Event	Criterion	Accuracy of landslide cells A1/(A1 + A3)	Accuracy of non-landsilde cells A4/(A2 + A4)	Accuracy of total cells (A1 + A4)/ (A1 + A2 + A3 + A4)[*]
2007 Krosa	Slope > 40 %, NDVI < 0, GI < 0.14	89.78 %	93.89 %	93.87 %
2009 Morakot	Slope > 40 %, NDVI < 0, GI < 0.14	62.44 %	95.48 %	93.70 %

[*] A1 is the number of landslide cells interpreted as landslide, A3 is the number of landslide cells not interpreted as landslide, A2 is the number of non-landslide cells interpreted as non-landslide, A4 is the number of non-landslide cells interpreted as landslide.
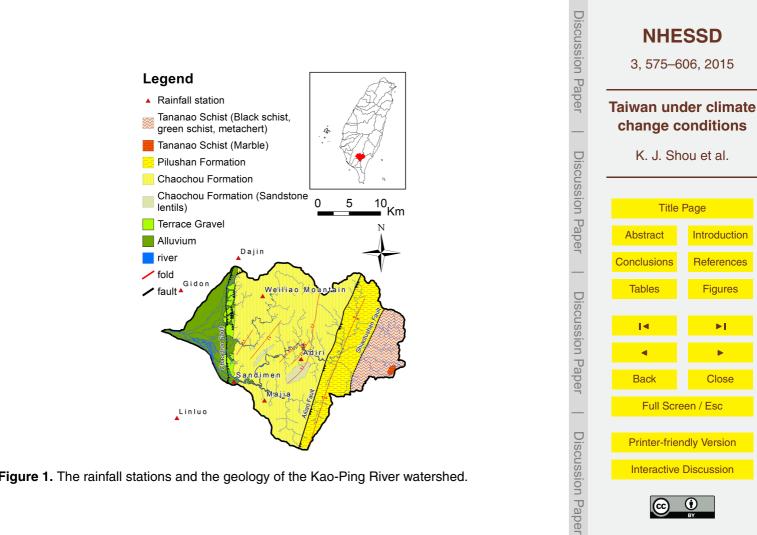
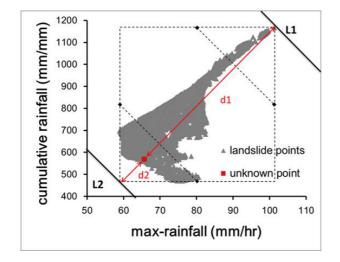**Figure 1.** The rainfall stations and the geology of the Kao-Ping River watershed.

Figure 2. The illustration of the landslide-rainfall index (I_d), defined by the distances d_1 and d_2 from the unknown point to the upper and lower linear thresholds as $d_1/(d_1 + d_2)$.

24hr Cumulative Rainfall of 10 Years Recurrent Period (mm)
High : 833.665
Low : 403.339

24hr Cumulative Rainfall of 20 Years Recurrent Period (mm)
High : 1071.5
Low : 449.626

24hr Cumulative Rainfall of 100 Years Recurrent Period (mm)
High : 1668.09
Low : 527.781

(a)10 year return period   (b)20 year return period   (c)100 year return period

Figure 3. The spatial distributions of 24 h accumulative rainfall for various return periods in the Kao-Ping River watershed.

Full Screen / Esc

Max Rainfall intensity of 10 Years Recurrent Period (mm/hr)
High : 145.066
Low : 69.9514

Max Rainfall intensity of 20 Years Recurrent Period (mm/hr)
High : 166.539
Low : 76.1393

Max Rainfall intensity of 100 Years Recurrent Period (mm/hr)
High : 256.765
Low : 91.106

(a)10 year return period

(b)20 year return period

(c)100 year return period

Figure 4. The spatial distributions of the maximum rainfall intensity for various return periods in the Kao-Ping River watershed.
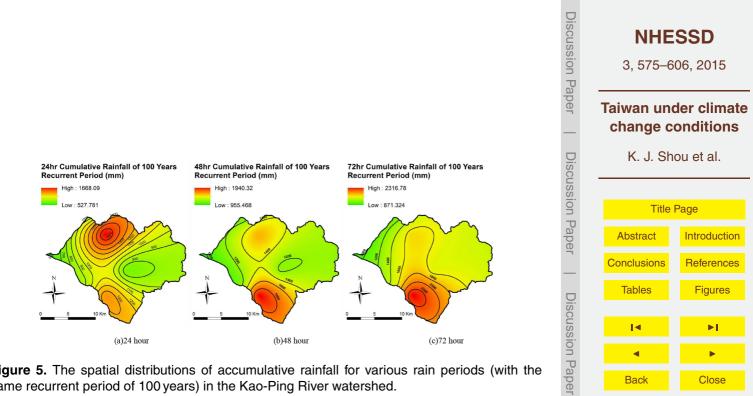
(a)24 hour   (b)48 hour   (c)72 hour

Figure 5. The spatial distributions of accumulative rainfall for various rain periods (with the same recurrent period of 100 years) in the Kao-Ping River watershed.

Figure 6. The predicted rainfall distributions in the Kao-Ping River watershed for the near future (2015–2039), based on the MRI-WRF dynamical downscaling data provided by TCCIP.
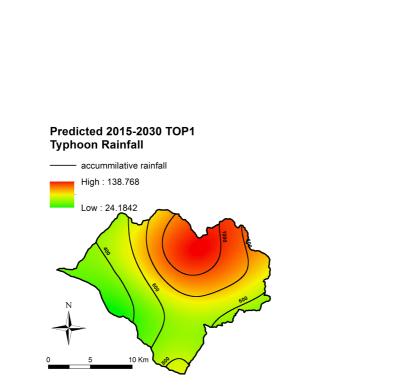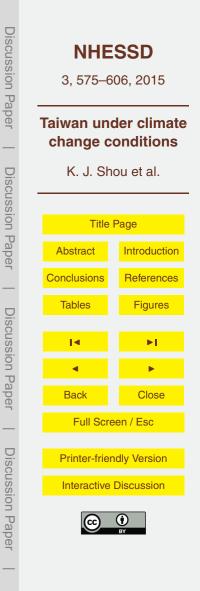
Figure 7. The predicted rainfall distributions in the Kao-Ping River watershed for the far future (2075–2099), based on the MRI-WRF dynamical downscaling data provided by TCCIP.

Figure 8. The data layers of the selected control factors in the Kao-Ping River watershed.

(b) 2009 Morakot

Figure 9. The landslide susceptibility maps obtained by the Instability Index method for 2007 Krosa Typhoon and 2009 Morakot Typhoon.

Figure 10. The landslide susceptibility maps obtained by the Logistic Regression analysis of 2007 Krosa Typhoon and 2009 Morakot Typhoon.

Full Screen / Esc

Typhoon Krosa
Landslide Suscepibility Map

landslide | High : 0.988726

Low : 0.00175494

N

0   5   10 Km

Typhoon Morakot
Landslide Suscepibility Map

landslde | High : 0.991858

Low : 0.00866157

N

0   5   10 Km

(b) 2009 Morakot

Figure 11. The ROC curves of the landslide susceptibility results by Instability Index method for 2007 Krosa Typhoon and 2007 Morakot Typhoon.

(a) 2007 Krosa

(b) 2009 Morakot

Figure 12. The ROC curves of the landslide susceptibility results by Logistic Regression method for 2007 Krosa Typhoon and 2007 Morakot Typhoon.

Full Screen / Esc

Printer-friendly Version

Interactive Discussion

Predicted Landslide Susceptbility Map, 24hr Cumulative Rainfall of 10 Years Recurrent Period

High : 0.992267

Low : 0.000592775

Predicted Landslide Susceptbility Map, 24hr Cumulative Rainfall of 20 Years Recurrent Period

High : 0.987106

Low : 0.000329924

Predicted Landslide Susceptbility Map, 24hr Cumulative Rainfall of 100 Years Recurrent Period

High : 0.989691

Low : 0.00235475

(a)10 year return period   (b)20 year return period   (c)100 year return period

Figure 13. The spatial distributions of landslide susceptibility with 24 h accumulative rainfall and rainfall intensity for various return periods in the Kao-Ping River watershed.

Predicted Landslide Susceptbility Map, 24hr Cumulative Rainfall of 100 Years Recurrent Period

High : 0.989691

Low : 0.00235475

N

0   5   10 Km

(a)24 hour

Predicted Landslide Susceptbility Map, 48hr Cumulative Rainfall of 100 Years Recurrent Period

High : 0.991207

Low : 0.000391228

N

0   5   10 Km

(b)48 hour

Predicted Landslide Susceptbility Map, 72hr Cumulative Rainfall of 100 Years Recurrent Period

High : 0.984857

Low : 0.000444359

N

0   5   10 Km

(c)72 hour

Figure 14. The spatial distributions of landslide susceptibility with 100 year return period for various rainfall periods in the Kao-Ping River watershed.

Full Screen / Esc

Predicted Landslide Susceptbility Map, 2015-2039 TOP1 Typhoon Rainfall

High : 0.99314

Low : 0.00640382

N

0   5   10 Km

(a) near future

Predicted Landslide Susceptbility Map, 2075-2099 TOP1 Typhoon Rainfall

High : 0.992803

Low : 0.00400605

N

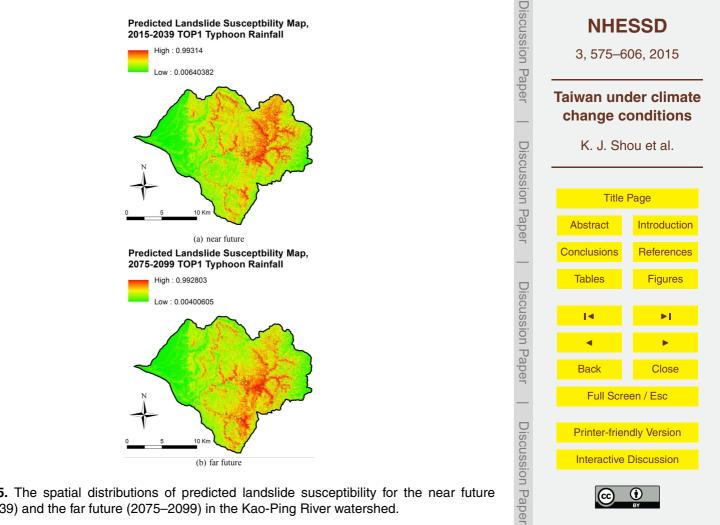0   5   10 Km

(b) far future

Figure 15. The spatial distributions of predicted landslide susceptibility for the near future (2015–2039) and the far future (2075–2099) in the Kao-Ping River watershed.